Structured doping of upconversion nanosystems for biological applications

Wang, Y.

Publication date
2011

CHAPTER 2

Upconversion Luminescence of

β-$NaYF_4$:Yb^{3+},Er^{3+}@β-$NaYF_4$ Core/Shell Nanoparticles

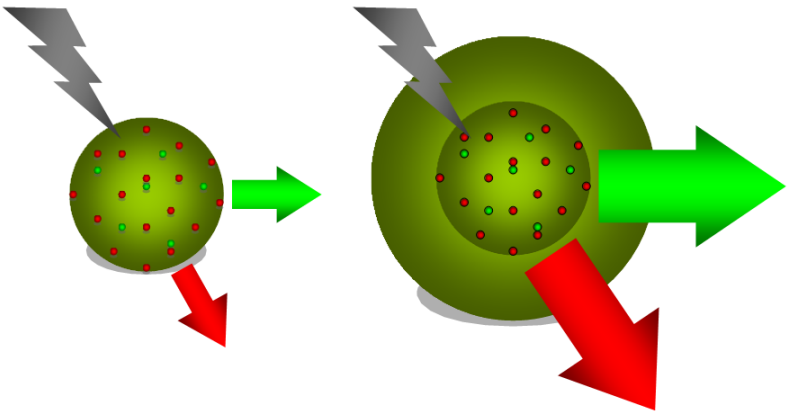

Abstract: Coating nanoparticles with a homogeneous layer outside the core has become a common method to improve the optical properties of nanoparticles. For rare earth ions doped nanoparticles a homogeneous coating is found to enhance the upconversion luminescence. However, so far a wide range of enhancements has been reported, which indicates that a fundamental picture of the enhancement mechanism is still lacking. In this work we have performed steady-state and time-resolved spectroscopic studies on one of the most efficient upconversion nanosystems - β-$NaYF_4$:Yb^{3+},Er^{3+} and β-$NaYF_4$:Yb^{3+},Er^{3+}@β-$NaYF_4$ core/shell nanoparticles. The role of the surface quench centers, typically the high-frequency vibrational modes provided by the organic surfactants in the upconversion luminescence, are studied in detail.

Our results show that the excitation power density, once over a threshold of ~150 W/cm^2, has a non-negligible annealing effect, which may even lead to high luminescence upconversion intensity of the core nanoparticles compared to the shell coated counterparts. The surface related high-frequency vibrational modes play an important role in the upconversion process as well as in the laser annealing process. The latter manifests itself in the difference of the laser annealing effect between the core and core/shell nanoparticles. From the upconversion luminescence kinetics analysis it turns out that the luminescent centers of the core nanoparticle are quenched to a large extent. Homogeneous coating can effectively reduce the quenching and enhance the upconversion luminescence. It is concluded that the upconversion emission spectrum, or more specifically, the ratio between the red and green emissions, can be greatly altered by excitation power density for core nanoparticles, but not for core/shell nanoparticles.

Keywords: upconversion · nanoparticle · vibrational mode · power density · core/shell structure · annealing

2.1 Introduction

In recent years, upconversion nanoparticles have attracted much attention because of their superior spectroscopic properties, which may used advantageously in many fields, especially in biology and biomedicine.[1] Amongst other advantages is the fact that excitation can be realized by a compact and inexpensive diode laser at near-infrared, e.g. 980 nm, which is within the optimal optics window of human tissue. In these biomedical applications upconversion efficiency is of critical importance since the sensitivity of labeling or the efficacy of the therapy relies on the luminescence of individual nanoparticles.

Hexagonal phase sodium yttrium fluoride (β-$NaYF_4$), known as the most efficient host material ever, has been widely studied recently.[2] In bulk, the low phonon energy of the host strongly suppresses multiphonon relaxation process in the emission centers, leading to a strong green upconversion emission ($^2H_{11/2}$, $^4S_{3/2} \rightarrow {}^4I_{15/2}$) and a very weak red upconversion emission ($^4F_{9/2} \rightarrow {}^4I_{15/2}$) at low doping level, because feeding of $^4F_{9/2}$, from which the red upconversion emission comes, requires phonon assistance to bridge the gaps of the order of several thousand cm^{-1}. Such gaps can not be efficiently bridged by the phonons of the host lattice that are of the order of several hundred cm^{-1}. When the size of the crystal decreases to the order of nanometers, it is generally observed that ratio between the red upconversion emission and the green one is (much) larger than in the bulk. This is usually ascribed to the presence of modes with high vibrational frequencies such as -OH, -CH, etc., which are provided by the organic surfactant molecules and match the energy gaps of the emission centers.[3] However, the underlying mechanism to date is still rather vague.

In order to enhance the emission, a core/shell structure has been generally adopted for nanoparticles, including rare earth ions doped nanocrystals, with the hope that the surface, and hence the quench centers, and emission centers would be separated in space. Both homogeneous and inhomogeneous core/shell structures have been synthesized and examined.[4] Typically, a homogeneous core/shell structure is favorable since this design can reduce the lattice mismatch between the core and the shell. Indeed, enhancement of down-conversion and upconversion luminescence has been observed for the core/shell nanoparticles.[2f,4k] The factor of enhancement is often given based on the experimental results under relatively high excitation radiation without taking into account possible laser-induced annealing.[5] One may expect, however, that the annealing dynamics are related with the surface-related vibrational properties since the annealing process is

basically thermodynamic in nature.

The situation introduced above encouraged us to perform the present research in order to illustrate the influence of the excitation power density and the surface properties on the upconversion dynamics of the rare earth ions doped in the nanoparticles, employing the most efficient upconversion system yet - β-$NaYF_4$:Yb^{3+},RE^{3+} nanoparticles and β-$NaYF_4$:Yb^{3+},RE^{3+}@β-$NaYF_4$ core/shell nanoparticles. Our results demonstrate that excitation power, once over ~150 W/cm^2, has a non-negligible annealing effect on the luminescence upconversion dynamics. Enhancement of the emission arising from the core/shell structure would be largely overestimated if this laser-induced annealing effect were not taken into account. In our case the luminescence upconversion intensity of the core can even exceed that of the core/shell ones subject to the same excitation power density at 980 nm. This "unusual" behavior is related to the high-frequency vibrational modes of the organic surfactant molecules, which contribute to the upconversion processes differently in the core and core/shell nanoparticles. From an analysis of the luminescence kinetics it becomes clear that luminescent centers, which are severely quenched in the core nanoparticle, can indeed be recovered by the homogeneous coating, and that the recovery effect depends on the shell thickness. It is concluded that the upconversion emission spectrum, e.g. the ratio between the red and green emissions, can be greatly altered by excitation power density for core nanoparticles, but not for core/shell nanoparticles.

2.2 Experiments

2.2.1 Chemicals

Rare earth oxides (RE = Y, Yb, Er), oleylamine (OM, >80%, *Acros*), oleic acid (OA, 90%), octadecene (ODE, 90%, *Acros*), trifluoroacetic acid (99%, *Acros*), CF_3COONa (>97%, *Acros*), ethanol, chloroform and hexane of analytical grade were purchased from *Beijing Chemicals* and used without further purification. Water used in the experiment was purified to a resistivity of 18.2MΩ.

2.2.2 Synthesis of β-$NaYF_4$:Yb^{3+},Er^{3+} nanoparticles and β-$NaYF_4$:Yb^{3+},Er^{3+}@β-$NaYF_4$ core/shell nanoparticles

The synthesis basically followed the routes previously reported in literature.[2a,2f,6] Briefly, rare earth trifluoroacetates $(CF_3COO)_3RE$ were prepared at beginning by dissolving rare earth oxides in trifluoroacetic acid (CF_3COOH), followed by drying at 60

°C. Sodium trifluoroacetate was prepared from sodium carbonate in a similar way. A mixture of designated molar ratio of CF_3COONa (2 mmol), $(CF_3COO)_3Y{\cdot}3H_2O$ (0.78 mmol), $(CF_3COO)_3Yb{\cdot}3H_2O$ (0.2 mmol), $(CF_3COO)_3Er{\cdot}3H_2O$ (0.02 mmol) powder were dissolved in 10 mL oleylamine (OM), and then filtered to get rid of the residues. Under vigorous stirring in a three neck flask, the mixture was then heated to 110 °C under the protection of a nitrogen or argon atmosphere and maintained at the same temperature for 30 minutes to remove the oxygen and residual water. Afterwards, the solution was totally clear with a slight yellow color. The mixture was then heated slowly to 300 °C in an argon atmosphere. After 30 min, 5 mL of the core product was taken out for reference. Reaction of the rest was continued for another 30 minutes with a slow addition of the shell precursors solution containing CF_3COONa (1 mmol), $(CF_3COO)_3Y{\cdot}3H_2O$ (0.5 mmol) in 5 mL OM. The final mixture was cooled down rapidly to room temperature. Both nanoparticles were then precipitated using ethanol and isolated via centrifugation for at least three times. The resulting nanoparticles were dried in vacuum at 60 °C for a minimum of 24 hours.

2.2.3 Characterizations

XRD studies were performed on powders using a Japan Rigaku D/max-rA X-ray diffractometer system with monochromatized Cu Kα radiation (λ = 1.5418 Å). The upconversion emission spectra were acquired using a Jobin-Yvon LabRam Raman spectrometer system equipped with holographic gratings of 1800 and 600 grooves/mm, respectively, and a Peltier air-cooled CCD detector. A 980 nm laser diode was used as the excitation source and the beam was either focused (about 8 cm focal length) to a spot size of approximately 0.2 mm in diameter to reach high excitation density or defocused to allow low density excitation. The upconversion luminescence kinetics was recorded with a 500 MHz Tektronix digital oscilloscope. Excitation was realized by a 10 Hz nanosecond optical parametric oscillator at 980 nm. Precise control of sample temperature (0.1 °C) was achieved by means of a Linkam THMS600 temperature programmable heating/cooling microscope stage. The THMS stage was used in conjunction with a Linkam LNP cooling system when cooling. In the excitation power dependent upconversion luminescence experiments, the power density was increased step by step.

2.3 Results and discussion

The powder X-ray diffraction (XRD) patterns (**Figure 2.1**) of the samples show

well-defined peaks, indicating the high crystallinity of the synthesized core and the core/shell structure nanoparticles. The diffraction peaks of β-$NaYF_4$:Yb^{3+},Er^{3+}@ β-$NaYF_4$ core/shell structure nanoparticles are slightly narrower than the XRD pattern of the core. Their peak positions and intensities of the XRD patterns match closely with that of hexagonal β-$NaYF_4$ in *JCPDF (28-1192)*. From the line broadening of the diffraction peaks the crystallite sizes of the samples are estimated to be approximately 13.9 nm for the core and 17.2 nm for the core/shell nanoparticles, respectively, based on the Debye-Scherrer formula. The volume ratio of the core and core/shell nanoparticles is about 1:1.9, which is consistent with the molar ratio of reaction materials (1:2). The cell parameters of the two samples were calculated by *Unitcell* with the crystal system, peak positions of XRD and corresponding crystal planes: a_c = 5.994 Å, c_c = 3.522 Å for core and $a_{c/s}$ = 5.973 Å, $c_{c/s}$ = 3.518 Å for core/shell nanoparticles, which are somewhat larger than the cell parameters of the bulk β-$NaYF_4$ (a = 5.960 Å, c = 3.510 Å) *(JCPDF 28-1192)*, indicating that the shell growing process has improved the crystallinity of the nanoparticles. Large size (~500 nm) β-$NaYF_4$ particles were synthesized following the same route for the mimic of bulk situation.

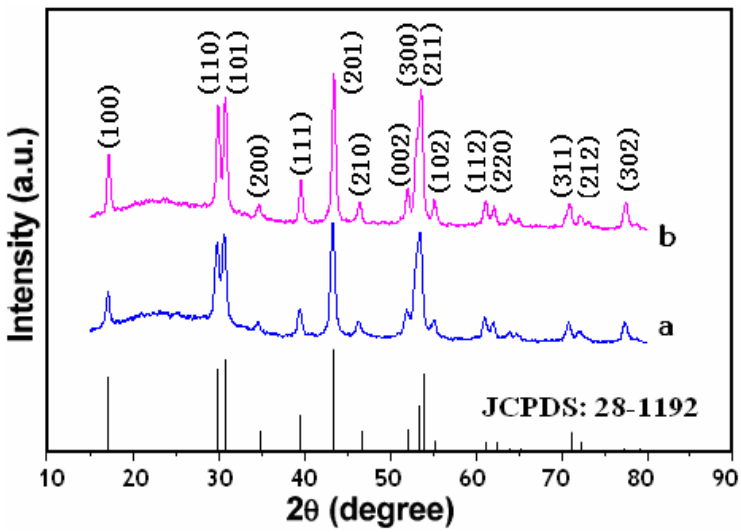

Figure 2.1. *XRD patterns of β-$NaYF_4$:Yb^{3+},Er^{3+} (a) and β-$NaYF_4$:Yb^{3+},Er^{3+}@ β-$NaYF_4$ core/shell (b) nanoparticles.*

When the β-$NaYF_4$:Yb^{3+},Er^{3+} nanoparticles are coated with β-$NaYF_4$ shells, the upconversion emission intensity is enhanced with respect to that of the core nanoparticles

under low excitation power density (see **Figure 2.2**). Here, low excitation power density is meant for the scenario that in this power region the upconversion spectrum is unique for a specific power density, regardless of its radiation history. Usually, this enhancement is attributed to the fact that a significant amount of nonradiative centers located on the surface of β-$NaYF_4$:Yb^{3+},Er^{3+} nanoparticles are eliminated by the β-$NaYF_4$ shell. Moreover, the distance between the luminescent rare earth ions and the surface quench centers in the core/shell structure is increased, which will reduce the nonradiative transition probabilities as well.

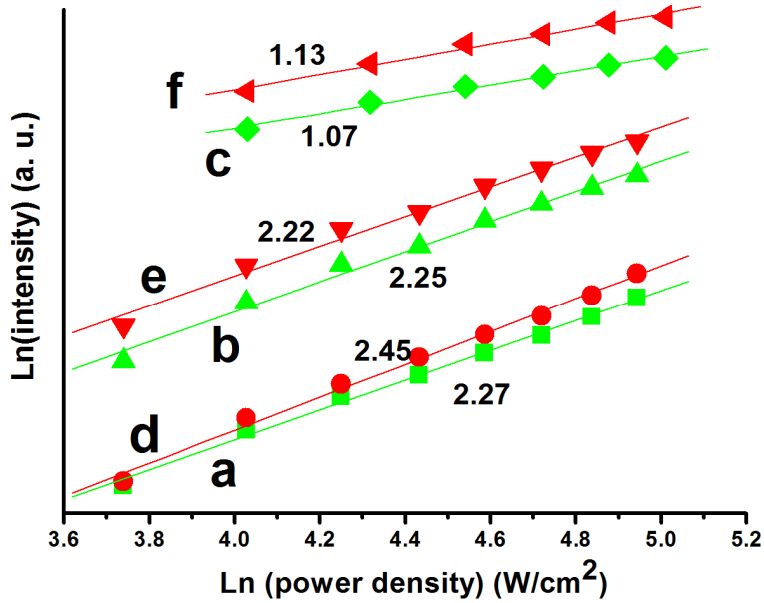

Figure 2.2. *Excitation power density dependence of 525, 545 nm green emissions ($^2H_{11/2}$/ $^4S_{3/2} \rightarrow {}^4I_{15/2}$) of core (a), core/shell (b), bulk counterpart (c) and 660 nm red emission ($^4F_{9/2} \rightarrow {}^4I_{15/2}$) of core (d), core/shell (e), bulk counterpart (f) at low power density (< 150 W/cm^2).*

At high Yb^{3+} concentration the upconversion processes for the red and green emission are depicted in **Figure 2.3**, from which it can be seen that the origin of the red emission is complex since three population routes co-exist for the $^4F_{9/2}$ level.

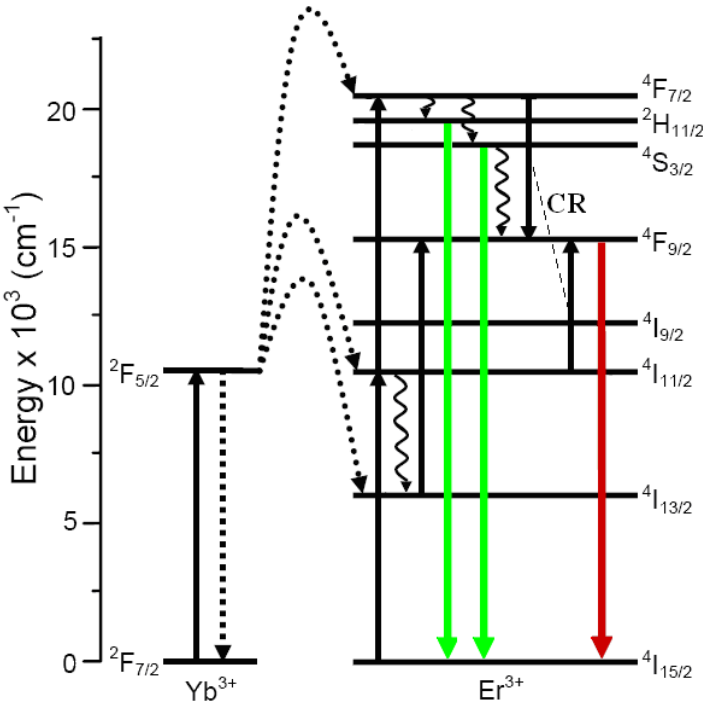

Figure 2.3. *Schematic illustration of the upconversion processes of Er^{3+} in β-$NaYF_4$:Yb^{3+},Er^{3+} under 980 nm excitation. CR: cross relaxation.*

In an upconversion mechanism (excited-state absorption (ESA) or energy-transfer upconversion (ETU)) where linear decay is dominant, the visible output intensity (I_V) will be proportional to some power (n) of the infrared excitation (I_{IR}) power at low excitation power density:[7]

$$I_V \propto I_{IR}^n$$

where n is the number of IR photons absorbed per visible photon emitted.

In our experiments n varies from 2.45 (core) to 2.22 (core/shell) for red emission and from 2.27 (core) to 2.25 (core/shell) for green emission This phenomenon manifests itself the involvement of processes other than ETU and/or ESA which should lead to n being not over 2. Considering the relatively high concentration of Er^{3+} (2 mol %) cross relaxation ($^2H_{11/2} \rightarrow {}^4F_{9/2}$ vs. $^4I_{11/2} \rightarrow {}^4F_{9/2}$) should occur here,[8] which might be responsible for the high n. This explanation, however, would seem to be at odds with the

observation that in a core/shell structure *n* is closer to 2, especially for red emission. This concern might be met by the following argument. Compared to the core nanoparticles, the influence of the high-frequency vibrational modes brought in by the surface organic groups will be much less in core/shell nanoparticles due to the space separation between the vibrational modes and the luminescent centers (*vide supra*). These vibrational modes are essential for the two population routes of the red emission (**Figure 2.3**). Indeed, for the bulk counterpart the upconversion red emission is very weak at low doping level.[9] However, one should not forget that the relatively high concentration of Yb^{3+} and Er^{3+} causes here a non-negligible cross relaxation process as evidenced by the strong red emission of the "bulk" sample (**Figure 2.3**). If a linear decay of the intermediate state is dominant, emission from $^2H_{11/2}/^4S_{3/2}$ and $^4I_{11/2}$ should exhibit, respectively, a quasi-quadratic and a quasi-linear excitation power dependence, and *n* should therefore be around 3. Otherwise *n* should be smaller and reach a minimum when the upconversion, instead of the linear decay, becomes dominant. The former scenario is similar to the case of core nanoparticles when nonradiative vibrational relaxation is very effective, whereas the latter one refers to core/shell nanoparticles where the surface related high-frequency vibrational modes do not affect greatly the luminescent centers due to the separation of the luminescent centers from the surface. This argument is supported by the fact that for the red emission *n* is the lowest for the "bulk" sample among the three samples. Note that the cross relaxation is not important for green emission and thus *n* does not vary much between the core and core/shell structures. This relationship can be used to change the color of the upconversion luminescence. In **Figure 2.4** the intensity ratio of red to green upconversion emissions demonstrates a dependence on the excitation power density and the nanostructure. For core nanoparticles the ratio is almost 1 at low excitation power density, but increases significantly with the excitation power density. This does not happen, however, for core/shell and the "bulk" samples where the ratio decreases only slightly with excitation power density. Therefore, the upconversion emission spectrum can be greatly modulated in the presence of an intermediate level with efficient nonradiative relaxation channels, as occurs, for example, in the case of core nanoparticles.

In the discussion so far we have not brought the effect of laser-induced thermal effects into consideration. In general, one should be cautious when trying to assess quantitatively the enhancement of the upconversion luminescence because various factors other than the separation between the surface quench centers and the luminescence centers might contribute to the enhancing mechanism. These include excitation power density dependence of the upconversion luminescence, laser induced annealing, and the fact that

unequal numbers of luminescent centers are excited in core/shell and core nanoparticles on account of their difference in size. Such factors are often neglected.

Highly doped sensitizer Yb^{3+} increases significantly the excitation absorption, and could thus lead to increased heating. To study the excitation power effect we compare two scenarios: low excitation power density as we have discussed so far, i.e., <150 W/cm^2 where the upconversion spectrum under lower excitation density can be recovered when the excitation power density decreases back to a low value, and high excitation power density, i.e., >150 W/cm^2, where the spectrum under lower excitation density can not be recovered when the excitation power density is decreased back.

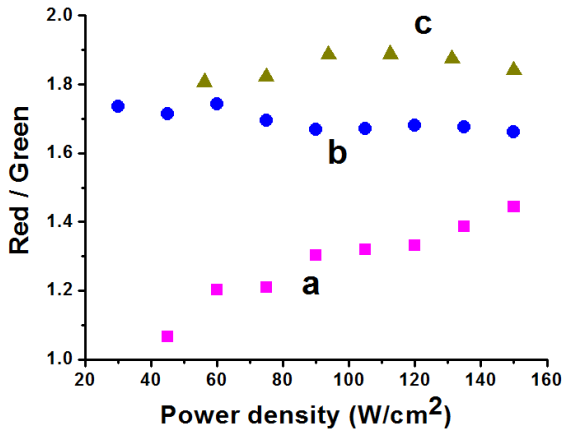

Figure 2.4. *Excitation power density dependence of the intensity ratio of red to green emissions for the core (a), core/shell nanoparticles (b) and bulk counterpart (c).*

In **Figure 2.5** the upconversion spectra in the two scenarios are shown for both the core and core/shell nanoparticles. It can be seen that at the lowest excitation power density applied in our experiment the upconversion emission of the core nanoparticles is weaker than that of the core/shell nanoparticles. This trend holds in the entire low-excitation power density region, but is reversed when the excitation power density is larger than ~ 200 W/cm^2 (**Figure 2.6**), in which case upconversion emission is stronger for the core than for the core/shell nanoparticles. Here the difference of Er^{3+} distribution between the two samples has been taken into account and calibrated. The behavior under high excitation power density is apparently related with an annealing effect since the upcoversion spectra of both samples can not be recovered when the excitation power comes back. Similar observations have been reported before.[10]

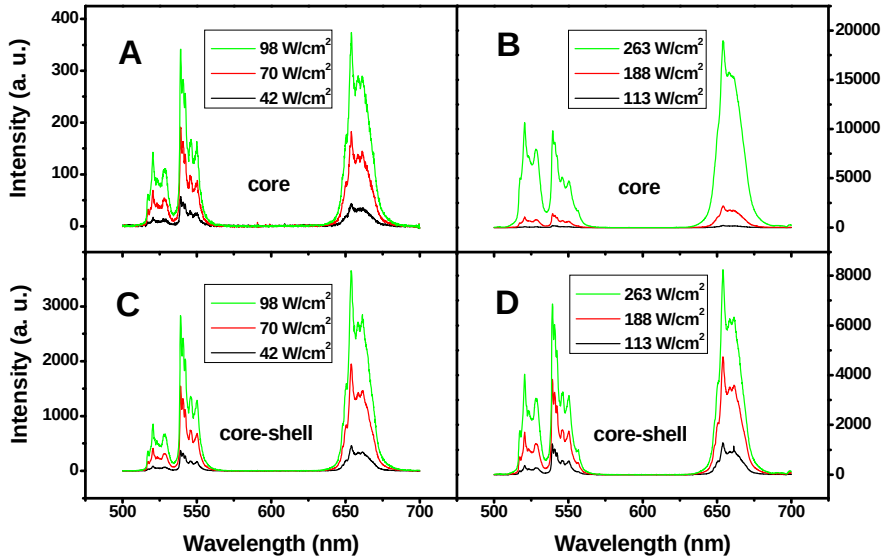

Figure 2.5. *The upconversion spectra of the core* **(A, B)** *and core/shell nanoparticles* **(C, D)** *under different NIR excitation power density.*

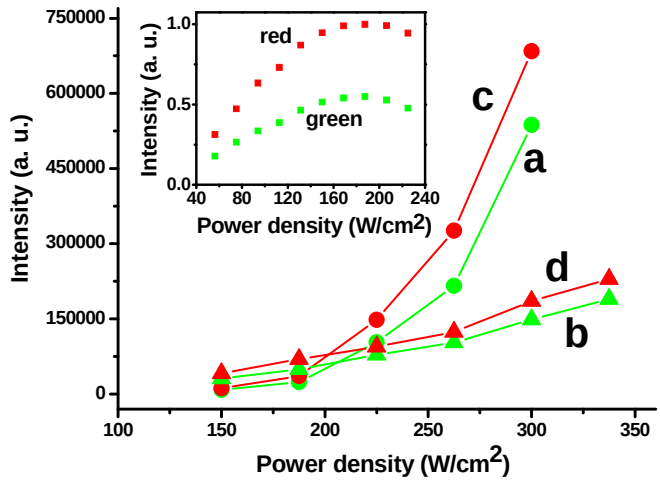

Figure 2.6. *525, 545 nm green emissions ($^2H_{11/2}$/ $^4S_{3/2}$→ $^4I_{15/2}$) of core (a) and core/shell (b) and 660 nm red emission ($^4F_{9/2}$→ $^4I_{15/2}$) of core (c) and core/shell (d) in high-power density regime.*

In order to understand the mechanism underlying these observations we have measured the local temperature of samples. As is well known, the close-lying $^2H_{11/2}$ and $^4S_{3/2}$ satisfy a Boltzmann distribution and the relevant emission intensity ratio can be used to label the local temperature of the luminescent centers.[11] The temperature dependence of green and red upconversion emission of β-$NaYF_4$:Yb^{3+},Er^{3+} and β-$NaYF_4$:Yb^{3+},Er^{3+}@β-$NaYF_4$ nanoparticles under a fixed excitation power density of about 110 W/cm^2 are shown in **Figure 2.7** and **Figure 2.8**. Therefore the radiation power density and the corresponding local temperature of the radiation area can be related, as has been done in **Table 2.1**. For core nanoparticles it is clear that at low excitation the temperature of the samples is not higher than ~100 °C, whereas at high excitation the induced temperature can be as high as >300 °C, causing serious annealing of the samples. One could wonder why the influence on the upconversion spectrum is not the same for the core and core/shell nanoparticles. To answer this question we have to consider the surface properties of the two samples. For core nanoparticles the excitation energy of Yb^{3+} ions can efficiently excite the surface-related high vibrational frequency modes which will then be transferred to the low-frequency lattice vibrational modes, increasing the lattice temperature. For the core/shell structure, on the contrary, the surface is separated by a shell from Yb^{3+} ions and the energy transfer channel of the excitation energy is thus blocked to a certain extent since the blocking effect depends on the quality of the shell. Thus the temperature increase in the core/shell nanoparticles will not be as clear as in the core nanoparticles under the same excitation power. The annealing naturally affects upconversion luminescence since it will lead to a more rigid structure, enhancing the upconversion emission (**Figure 2.6**). If the annealing effect is significant, the upconversion spectrum after excitation with high power density is expected to be different from the spectrum before excitation. This is indeed what is observed, i.e., when the excitation power density is >150 W/cm^2 (≈100 °C) the upconversion spectrum can not be recovered.

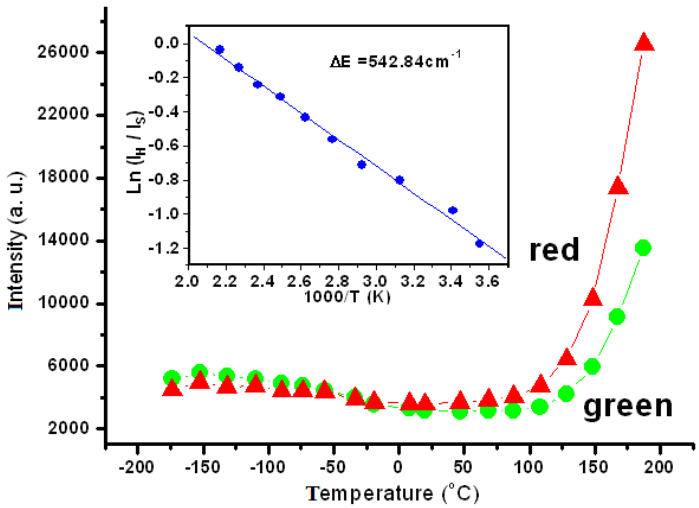

Figure 2.7. *Temperature dependence of green and red upconversion emission of β-$NaYF_4$:Yb^{3+},Er^{3+} nanoparticles under a fixed excitation power density of about 110 W/cm^2. (inset: temperature dependence of the intensity ratio of $^2H_{11/2}$ → $^4I_{15/2}$ and $^4S_{3/2}$ → $^4I_{15/2}$ of β-$NaYF_4$:Yb^{3+},Er^{3+} nanoparticles).*

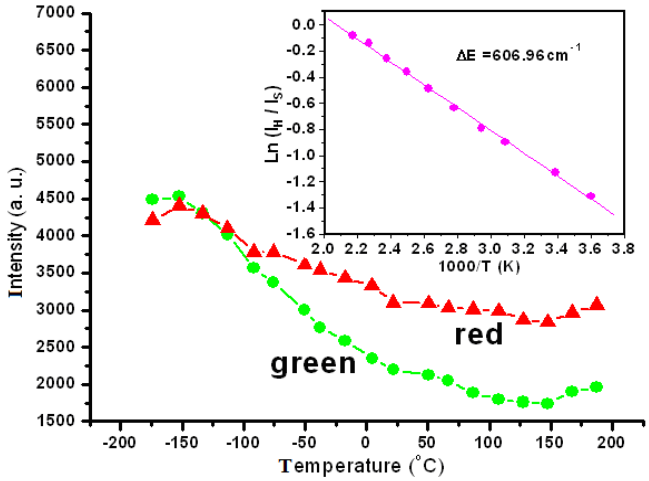

Figure 2.8. *Temperature dependence of green and red upconversion emission of β-$NaYF_4$:Yb^{3+},Er^{3+}@β-$NaYF_4$ core-shell nanoparticles under a fixed excitation power density of about 110 W/cm^2. (inset: temperature dependence of the intensity ratio of $^2H_{11/2}$ → $^4I_{15/2}$ and $^4S_{3/2}$ → $^4I_{15/2}$ of β-$NaYF_4$:Yb^{3+},Er^{3+}@β-$NaYF_4$ nanoparticles).*

Table 2.1. *Excitation power density and the corresponding local temperature of the core and core/shell nanoparticles.*

	Low power density				High power density				
Power density (W/cm^2)	60	90	120	150	187.5	225	262.5	300	337.5
Core temperature (°C)	31.4	54.8	76.7	100.1	157.4	199.6	239.8	274.9	324.0
Core/shell temperature (°C)	15.3	27.6	40.3	52.5	72.2	94.0	115.1	136.9	158.3

Finally, we would like to discuss the time behavior of the upconversion spectra at the two excitation power levels. **Figure 2.9** depicts the time evolution of the upconversion luminescence of the core and core/shell nanoparticles and the "bulk" samples. Rise and decay components are observed similar to other reports.[12] All curves can be well fitted with the following equation:

$$I(t) = -Ae^{-t/\tau_r} + B_1 e^{-t/\tau_1} + B_2 e^{-t/\tau_2}$$

where A and B_1 and B_2 are all positive parameters. The assumption of a single rise component is simply due to limitation of the time resolution of the setup. In analysing the curves one has to realize that luminescence decay does not always represent the depopulation of the emissive state, and that similarly luminescence rise does not always represent the population of the emissive state. This is due to the fact that when a rise and a decay component coexist in luminescence kinetics, decay is always the longer one, even if population is slower than depopulation. *Upconversion luminescence of rare earth ions is precisely one of these examples*. Since the intermediate states mediate the upconversion process, e.g., $^4I_{11/2}$ and $^4I_{13/2}$ have much longer lifetimes relative to the final upconversion emission states, e.g., $^4S_{3/2}$ (for green emission) and $^4F_{9/2}$ (for red emission), the rise components in our measurements are determined by the lifetimes of the latter states, whereas the intermediate states, i.e., $^4I_{11/2}$ and/or $^4I_{13/2}$, determine the decay components of the upconversion luminescence kinetics. Therefore τ_1 and τ_2 in fact reflect mainly the nature of $^4I_{11/2}$ and $^4I_{13/2}$ states, and τ_r represents the lifetime of the $^4S_{3/2}$ or $^4F_{9/2}$.

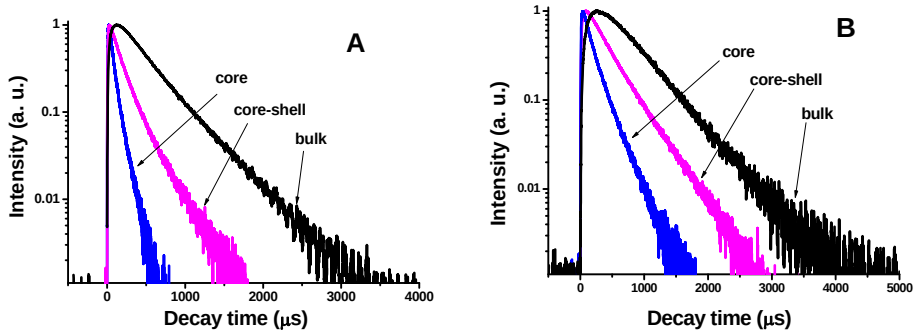

Figure 2.9. *Temporal behavior of the green* **(A)** *and red* **(B)** *upconversion luminescence of the core, core/shell nanoparticles and counterpart bulk β-$NaYF_4$:Yb^{3+},Er^{3+}.*

Table 2.2. *Rise and decay times of green and red emission of core, core-shell nanoparticles and the bulk counterpart.*

	$^4S_{3/2} \rightarrow {}^4I_{15/2}$ (green emission)			$^4F_{9/2} \rightarrow {}^4I_{15/2}$ (red emission)		
	Core	Core / Shell	Bulk	Core	Core / Shell	Bulk
Rise time (μs)	7.0 ± 0.2	8.9 ± 0.4	40.0 ± 1.0	13.8 ± 0.4	29.3 ± 1.0	136.3 ± 0.1
Decay time (μs)	τ_1 = 39.2 ± 0.5 (64.3%)	τ_1 = 128.7 ± 0.9 (78.8%)	406.3 ± 1.5	τ_1 = 87.5 ± 1.6 (48.0%)	τ_1 = 342.0 ± 1.7 (91.8%)	492.7 ± 0.1
	τ_2 = 92.7 ± 0.6 (35.7%)	τ_2 = 302.4 ± 2.1 (21.2%)		τ_2 = 222.4 ± 1.1 (52.0%)	τ_2 = 511.0 ± 13.0 (8.2%)	

The fit results are given in **Table 2.2**. The decay time constant of the green emission ($^4S_{3/2} \rightarrow {}^4I_{15/2}$) increases from ~ 7 μs for the core to ~ 9 μs for the core/shell to ~ 40 μs for the "bulk". Clearly, the core/shell structure differs from the core in removing the surface effect. This difference might be understood as follows: the core/shell structure separates in space the surface from the luminescent centers, which can (i) to a certain extent block the excitation energy transportation to quench centers on the surface, and (ii) recover the surface luminescent centers, which are severely quenched in the core. Moreover, the multiphonon relaxation processes in the luminescent centers mediated by the surface-related organic high vibrational frequency modes will be different. The core/shell structure increases the distance between the luminescent centers and the surfactants that provide the vibrational modes responsible for nonradiative vibrational

relaxation. As a result, the interaction between the two is reduced, and nonradiative vibrational relaxation becomes inefficient.

The discussion above leads to the conclusion that the lifetimes in core/shell nanoparticles are shorter than in the bulk, although they are longer than those of the core nanoparticles, the actual increase depending on the shell thickness. Simultaneously *n* will decrease resulting from the evolution from linear-decay dominant to upconversion dominant.

2.4 Conclusions

Steady-state and time-resolved spectroscopic studies have been performed on one of the most efficient upconversion nanosystems – β-$NaYF_4$:Yb^{3+},Er^{3+} and β-$NaYF_4$:Yb^{3+},Er^{3+}@β-$NaYF_4$ core/shell nanoparticles. It has been found that excitation power and surface properties - typically the high-frequency vibrational modes provided by the organic surfactants during the synthetic process - affect the luminescence upconversion dynamics.

Our results show that excitation power, once over a certain threshold, e.g. ~150 W/cm^2 in the present case, has a non-negligible annealing effect. The surface-related high frequency vibrations play an important role in the upconversion process as well as in the laser induced annealing process in the core and core/shell nanoparticles. From an analysis of the luminescence kinetics it has become clear that a large number of luminescent centers of the core nanoparticle are severely quenched, but can be recovered by homogeneous coating. It is concluded that for core nanoparticles the upconversion emission spectrum can be changed to a large extent by the excitation power density but not for core/shell nanoparticles.

2.5 Acknowledgments

This work was supported by NSFC of China (60771051, 60601015, 10674132, 10874179 and 20603035), and the exchange program between CAS of China and KNAW of the Netherlands.

2.6 References

1 (*a*) Up-Converting Phosphor Reporters for Nucleic Acid Microarrays. F. van de Rijke, H. Zijlmans, S. Li, T. Vail, A.K. Raap, R.S. Niedbala, and H.J. Tanke; *Nat. Biotechnol.* **2001**, *19*, 273-276; (*b*) In Vivo and Scanning Electron Microscopy Imaging of Upconverting Nanophosphors in Caenorhabditis elegans. S.F. Lim, R. Riehn, W.S. Ryu, N. Khanarian, C.K. Tung, D. Tank, and R.H. Austin; *Nano Lett.,* **2006**, *6*, 169-174; (*c*) Green Upconversion Nanocrystals for DNA Detection. L.Y. Wang, Y.D. Li; *Chem. Commun*., **2006**, *24*, 2557-2559; (*d*) Versatile Photosensitizers for Photodynamic Therapy at Infrared Excitation. P. Zhang, W. Steelant, M. Kumar, and M. Scholfield; *J. Am. Chem. Soc.,* **2007**, *129*, 4526-4527; (*e*) Design of a Highly Sensitive and Specific Nucleotide Sensor Based on Photon Upconverting Particles. P. Zhang, S. Rogelj, K. Nguyen, and D. Wheeler; *J. Am. Chem. Soc.,* **2006**, *128*, 12410-12411; (*f*) High Contrast in Vitro and in Vivo Photoluminescence Bioimaging Using Near Infrared to Near Infrared Up-Conversion in Tm^{3+} and Yb^{3+} Doped Fluoride Nanophosphors. M. Nyk, R. Kumar, T.Y. Ohulchanskyy, E.J. Bergey, and P.N. Prasad; *Nano Lett.,* **2008**, *8*, 3834-3838.

2 (*a*) Synthesis of Colloidal Upconverting $NaYF_4$ Nanocrystals Doped with Er^{3+}, Yb^{3+} and Tm^{3+}, Yb^{3+} via Thermal Decomposition of Lanthanide Trifluoroacetate Precursors. J.C. Boyer, F. Vetrone, L.A. Cuccia, and J.A. Capobianco; *J. Am. Chem. Soc.,* **2006**, *128*, 7444-7445; (*b*) A Strategy to Protect and Sensitize Near-Infrared Luminescent Nd^{3+} and Yb^{3+}: Organic Tropolonate Ligands for the Sensitization of Ln^{3+}-Doped $NaYF_4$ Nanocrystals. J. Zhang, C.M. Shade, D.A. Chengelis, and S. Petoud; *J. Am. Chem. Soc.,* **2007**, *129*, 14834-14835; (*c*) Lanthanide-Doped $NaYF_4$ Nanocrystals in Aqueous Solution Displaying Strong Up-Conversion Emission. H. Schafer, P. Ptacek, K. Kompe, M. Haase; *Chem. Mater.,* **2007**, *19*, 1396-1400; (*d*) Synthesis of Oil-Dispersible Hexagonal-Phase and Hexagonal-Shaped $NaYF_4$:Yb,Er Nanoplates. Y. Wei, F. Lu, X. Zhang, and D. Chen; *Chem. Mater.,* **2006**, *18*, 5733-5737; (*e*) Synthesis, Characterization, and Biological Application of Size-Controlled Nanocrystalline $NaYF_4$:Yb,Er Infrared-to-Visible Up-Conversion Phosphors. G. Yi, H. Lu, S. Zhao, Y. Ge, W. Yang, D. Chen, and L.H. Guo; *Nano Lett.,* **2004**, *4*, 2191-2196; (*f*) Highly Efficient Multicolor Up-Conversion Emissions and Their Mechanisms of Monodisperse $NaYF_4$:Yb,Er Core and Core/Shell -Structured Nanocrystals. H.X. Mai, Y.W. Zhang, L.D. Sun, and C.H. Yan; *J. Phys. Chem. C,* **2007**, *111*, 13721-13729; (*g*) High-Quality Sodium Rare-Earth Fluoride Nanocrystals: Controlled Synthesis and Optical Properties. H.X. Mai, Y.W. Zhang, R. Si, Z.G. Yan, L.D. Sun, L.P. You, and C.H. Yan; *J. Am. Chem. Soc.,* **2006**, *128*, 6426-6436; (*h*) Controlled Synthesis and Luminescence of Lanthanide Doped $NaYF_4$ Nanocrystals. L. Wang, Y. Li; *Chem. Mater.,* **2007**, *19*, 727-734; (*i*) Highly Uniform and Monodisperse β-$NaYF_4$:Ln^{3+} (Ln = Eu, Tb, Yb/Er, and Yb/Tm)

Hexagonal Microprism Crystals: Hydrothermal Synthesis and Luminescent Properties. C. Li, Z. Quan, J. Yang, P. Yang, and J. Lin ; *Inorg. Chem.,* **2007**, *46*, 6329-6337; (*j*) Controlled Synthesis, Formation Mechanism, and Great Enhancement of Red Upconversion Luminescence of $NaYF_4$:Yb^{3+}, Er^{3+} Nanocrystals/Submicroplates at Low Doping Level. J.W. Zhao, Y.J. Sun, X.G. Kong, L.J. Tian, Y. Wang, L.P. Tu, J.L. Zhao, and H. Zhang; *J. Phys. Chem. B*, **2008**, *112*, 15666-15672.

3 (*a*) Improvement in the Luminescence Properties and Processability of LaF_3/Ln and $LaPO_4$/Ln Nanoparticles by Surface Modification. J.W. Stouwdam, and F.C.J.M. van Veggel; *Langmuir,* **2004**, *20*, 11763-11771; (*b*) Lanthanide(III)-Doped Nanoparticles That Emit in the Near-Infrared. G. A. Hebbink, J.W. Stouwdam, D.N. Reinhoudt, F.C.J.M. van Veggel, *Adv. Mater.,* **2002**, *14*, 1147-1150.

4 (*a*) A Facile Synthesis and Photoluminescent Properties of Redispersible CeF3, CeF_3:Tb^{3+}, and CeF_3:Tb^{3+}/LaF_3 (Core/Shell) Nanoparticles. Z.L. Wang, Z.W. Quan, P.Y. Jia, C.K. Lin, Y. Luo, Y. Chen, J. Fang, W. Zhou, C.J. O'Connor, and J. Lin; *Chem. Mater.,* **2006**, *18*, 2030-2037; (*b*) Epitaxial Synthesis of Uniform Cerium Phosphate One-Dimensional Nanocable Heterostructures with Improved Luminescence. W.B. Bu, Z.L. Hua, H.R. Chen, and J.L. Shi; *J. Phys. Chem. B*, **2005**, *109*, 14461-14464; (*c*) Synthesis of Eu^{3+}-Doped Core and Core/Shell Nanoparticles and Direct Spectroscopic Identification of Dopant Sites at the Surface and in the Interior of the Particles. O. Lehmann, K. Kömpe, and M. Haase; *J. Am. Chem. Soc.,* **2004**, *126*, 14935-14942; (*d*) Surface Modification of ZrO_2:Er^{3+} Nanoparticles to Attenuate Aggregation and Enhance Upconversion Fluorescence. Q. Lü, F.Y. Guo, L. Sun, A.H. Li, and L.C. Zhao; *J. Phys. Chem. C*, **2008**, *112*, 2836-2844; (*e*) LaF_3, CeF_3, CeF_3:Tb^{3+}, and CeF_3:Tb^{3+}@LaF_3 (Core−Shell) Nanoplates: Hydrothermal Synthesis and Luminescence Properties. C.X. Li, X.M. Liu, P.P. Yang, C.M. Zhang, H.Z. Lian, and J. Lin; *J. Phys. Chem. C*, **2008**, *112*, 2904-2910; (*f*) Effects of the Coating Process on Nanoscale Y_2O_3:Eu^{3+} Powders. Q. Li, L. Gao, and D.S. Yan; *Chem. Mater.,* **1999**, *11*, 533-535; (*g*) Luminescence Enhancement by Energy Transfer in Core-Shell Structures. C. Louis, S. Roux, G. Ledoux, C. Dujardin, O. Tillement, B.L. Cheng, and P. Perriat; *Chem. Phys. Lett*., **2006**, 429, 157-160; (*h*) Luminescent Enhancement in Europium-doped Yttria Nanotubes Coated with Yttria. X. Bai, H.W. Song, G.H. Pan, Z.X. Liu, S.Z. Lu, W.H. Di, X.G. Ren, Y.Q. Lei, Q.L. Dai, and L.B. Fan; *Appl. Phys. Lett.,* **2006,** *88*, 143104; (*i*) Facile Sonochemical Synthesis of $CePO_4$:Tb/$LaPO_4$ Core/Shell Nanorods with Highly Improved Photoluminescent Properties. L. Zhu, X.M. Liu, X.D. Liu, Q. Li, J.Y. Li, S.Y. Zhang, J. Meng, and X.Q. Cao; *Nanotechnology,* **2006,** *17,* 4217; (*j*) Green-Emitting $CePO_4$:Tb/$LaPO_4$ Core–Shell Nanoparticles with 70% Photoluminescence Quantum Yield. K. Kömpe, H. Borchert, J. Storz, A. Lobo, S. Adam, T. Möller, and M. Haase;.*Angew. Chem. Int. Ed.,* **2003**, *42*, 5513-5516; (*k*) Water-Soluble $NaYF_4$:Yb,Er(Tm) /$NaYF_4$/Polymer Core/Shell/Shell Nanoparticles with Significant

Enhancement of Upconversion Fluorescence. G.S. Yi, G.M. Chow; *Chem. Mater.,* **2007**, 19, 341-343.

5 IR-Annealing Technology for Glass Products. V.E. Tyutyunnik, and Y.A. Guloyan; *Glass and Ceramics*, **2000**, *57*, Nos. 7-8.

6 Synthesis of Hexagonal-Phase $NaYF_4$:Yb,Er and $NaYF_4$:Yb,Tm Nanocrystals with Efficient Up-Conversion Fluorescence. G.S. Yi, and G.M. Chow; *Adv. Funct. Mater.,* **2006**, *16*, 2324-2329.

7 Power Dependence of Upconversion Luminescence in Lanthanide and Transition-Metal-Ion Systems. M. Pollnau, D.R. Gamelin, S.R. Lüthi, and H.U. Güdel; *Phys. Rev. B*, **2000**, *61*, 3337-3346.

8 Tunable Red-Green Upconversion Luminescence in Novel Transparent Glass Ceramics Containing Er: $NaYF_4$ Nanocrystals. F. Liu, E. Ma, D.Q. Chen, Y.L. Yu, and Y.S. Wang; *J. Phys. Chem. B*, **2006**, 110, 20843-20846.

9 Significance of Yb^{3+} Concentration on the Upconversion Mechanisms in Codoped Y_2O_3:Er^{3+}, Yb^{3+} Nanocrystals. F. Vetrone, J.C. Boyer, J.A. Capobianco, A. Speghini, and M. Bettinelli*; J. Appl. Phys.,* **2004**, *96*, 661-667.

10 (*a*) Size-Dependent Upconversion Luminescence in Er^{3+}/Yb^{3+}-Codoped Nanocrystalline Yttria: Saturation and Thermal Effects. X. Bai; H.W. Song, G.H. Pan, Y.Q. Lei, T. Wang, X.G. Ren, S.Z. Lu, B. Dong, Q.L. Dai, and L.B. Fan; *J. Phys. Chem. C*, **2007**, *111*, 13611-13617; (*b*) Unusual Power-Dependent and Time-Dependent Upconversion Luminescence in Nanocrystals Y_2O_3: Ho^{3+}/Yb^{3+}. L.M. Yang, H.W. Song, L.X. Yu, Z.X. Liu, and S.Z. Lu; *Journal of Luminescence,* **2006**, *116*, 101-106.

11 Effect of Annealing on Upconversion Luminescence of ZnO:Er^{3+} Nanocrystals and High Thermal Sensitivity. X. Wang, X.G. Kong, Y. Yu, Y.J. Sun, and H. Zhang; *J. Phys. Chem. C,* **2007**, *111*, 15119-15124.

12 Dynamics of Infrared-to-Visible Upconversion in $Cs_3Lu_2Br_9$:1%Er^{3+}. M.P. Hehlen, G. Frei, and H.U. Güdel; *Phys. Rev. B,* **1994,** *50*, 16264-16273.